Kinetic models for synaptic vesicle release

Schotten, S.

2016

document version
Publisher's PDF, also known as Version of record

CHAPTER 5

Reduction of the energy barrier for synaptic vesicle fusion during short-term synaptic plasticity

Sebastiaan Schotten[1,*], Marieke Meijer[1,*], Matthijs Verhage[1], L. Niels Cornelisse[1]

[1]Department of Functional Genomics, Center for Neurogenomics and Cognitive Research, Neuroscience Campus Amsterdam, Vrije Universiteit (VU) Amsterdam and VU Medical Center, 1081HV Amsterdam, The Netherlands

[*] these authors contributed equally to this study

Abstract

Short-term synaptic plasticity (STP) is essential for information processing and working memory. Post-tetanic potentiation (PTP) induced by high-frequency stimulation (HFS) is thought to depend on residual Ca^{2+}-dependent changes in release probability, but has also been linked to activity-dependent alterations to the readily releasable pool (RRP) and facilitation of Ca^{2+} currents. The dominant biophysical mechanism underpinning PTP, however, remains elusive. In this study, we investigate the magnitude of an alternative and largely overlooked source of PTP: the modulation of the energy barrier for synaptic vesicle fusion by residual Ca^{2+}. We apply a mathematical model for hypertonic sucrose (HS)-induced vesicle release to simultaneously assess the RRP size and the release rate constant from HS-stimuli before and after a high-frequency action potential train. Our analysis reveals that while 5 seconds after HFS the RRP was recovered to only 70% of its resting size, the vesicular release probability (p_{vr}) was potentiated by 32% with a concomitant 21% potentiation of the release rate constant for 0.5M HS, corresponding to a 0.2RT drop in fusion energy barrier height. However, this lowered fusion energy barrier during PTP turns out not to correlate significantly with the increase in p_{vr}. To investigate the role of Synaptotagmin-1 (Syt-1) in fusion energy barrier modulation during PTP, we repeat these experiments on Syt-1 KO neurons. We find a stronger 93% potentiation in p_{vr} but a 27% potentiation of the release rate constant for 0.5M HS, similar to WT, corresponding to a 0.2RT drop in fusion energy barrier height. Therefore, we conclude that the reduction of the fusion energy barrier during PTP does not require Syt-1.

5.1 Introduction

For important brain functions, such as information processing and working memory, synapses need to adapt their synaptic strength at the millisecond to minute timescale in response to neuronal activity [9]. This short-term synaptic plasticity (STP) is dominated by presynaptic processes, in contrast to long-term plasticity, which occurs on much longer timescales (minutes up to years) and involves mainly post-synaptic regulation [17]. Synaptic strength is presynaptically determined by the number of vesicles that are ready to be released (i.e. primed) and by the vesicular release probability (p_{vr}), which is the chance for a vesicle to be released during an action potential (AP). Ca^{2+} plays a prominent role in the regulation of both of these synaptic parameters [46–48]. Many intracellular pathways have been identified that modulate STP when activated by residual Ca^{2+} that accumulates during high-frequency stimulation (HFS) [57].

Reduction of synaptic strength during HFS, known as short-term depres-

sion, can be understood by a depletion of vesicles in the readily releasable pool (RRP). However, the mechanisms underpinning facilitation and post-tetanic potentiation (PTP) have remained enigmatic. In general, synapses with initial low release probability facilitate by increasing their release probability during HFS [79]. Different mechanisms such as Ca^{2+} current facilitation, buffer saturation, increased priming, and increased quantal size have been proposed for different types of synapses, but explain only partly the amount of synaptic potentiation observed in these synapses [47, 204, 205]. While the decay of PTP and of residual Ca^{2+} were found to follow the same time course, it remains an unresolved question what the dominant mechanism is that produces short-term potentiation in response to elevated residual Ca^{2+} [47, 55, 56].

A potential mechanism that has received relatively little attention is the possibility for residual Ca^{2+} to modulate the energy barrier for synaptic vesicle fusion. Mixing of lipid membranes requires substantial energy and vesicles have to overcome this energy barrier before they can fuse and release they neurotransmitter content [91]. The fast Ca^{2+} sensors Synaptotagmin-1, -2 and -9, which synchronize vesicle release with an AP-induced Ca^{2+} influx, lower the fusion energy barrier very rapidly [30, 76, 140, 141]. The potential mechanism underpinning residual Ca^{2+}-dependent reduction of the fusion energy barrier should operate on a timescale much slower than that of the fast Ca^{2+} sensors (in the order of seconds, for PTP). Other presynaptic proteins, such as Complexin, Munc13, Syntaxin-1, and Munc18 also have been shown to modulate the fusion energy barrier and affect STP [84, 87, 109, 110, 144]. In the absence of a method to quantify changes in energy barrier height, the contribution of a fusion energy barrier modulation to STP has been noted, but not quantified [55, 56].

Here we use our previously presented method (see [187]) to quantify both changes in RRP size and changes in the fusion energy barrier height from synaptic responses induced by hypertonic sucrose stimulation, to investigate their respective contributions to PTP. We show that while the RRP is not fully recovered 5 seconds after HFS, p_{vr} is enhanced, and the fusion energy barrier is reduced. This reduction however does not correlate significantly with the increase in p_{vr}. Finally, we show that all these HFS-induced phenomena cannot be attributed to a higher activation of the Ca^{2+} sensor due to accumulation of residual Ca^{2+} during HFS, since a similar potentiation of release and a concomitant decrease of the energy barrier remain in the absence of Synaptotagmin-1.

5.2 Results

5.2.1 The fusion energy barrier is reduced after high frequency stimulation

First, we compared the charge of an AP-induced EPSC before and 5 seconds after HFS (fig. 5.1A). While some cells showed a clear potentiation of the EPSC after HFS, others displayed a reduction (fig. 5.1B). On average, the EPSC was not changed 5 seconds after HFS. To investigate the role of priming and energy barrier modulation in PTP, we applied our method of fitting HS-induced synaptic responses to simultaneously quantify RRP size and release kinetics before and after HFS (100 AP at 40 Hz). Despite full recovery of AP-evoked EPSCs 5 seconds after RRP depletion by HFS, none of the cells, including those that showed potentiation of the AP induced EPSC, showed a complete RRP recovery,

Figure 5.1 ***(facing page)*****:** *PTP involves a significant increase in both release probability and release rate constant.* (A) Top: stimulation protocol. The 0.5 Hz stimuli were administered 10 times before and 5 s after HFS, and the EPSC evoked by the first of each of these low-frequency trains was used to determine the AP-evoked charge. Bottom: typical examples of action potential-evoked release, pre- and post-HFS. (B) Charge of AP-evoked EPSCs (integrated over 100 ms) is not significantly changed after HFS (Pre-HFS: 229 ± 35 pC, n = 24; Post-HFS: 210 ± 34 pC, n = 24; p = 0.22, paired t-test). (C) RRP size, measured by 0.5M HS, is reduced 5 s after HFS (Pre-HFS: 3.26 ± 0.55 nC, n = 26; Post-HFS: 2.29 ± 0.38 nC, n = 26; $p = 6.7 \cdot 10^{-5}$, paired t-test). (D) Inset: stimulation protocol for comparison of HS-induced release before and 5 s after HFS. Bottom: typical example of EPSCs evoked by application of 0.25M (grey) and 0.5M (black) HS to WT neurons, pre- (left) and post-HFS (right). Note the relative increase of release triggered by the 0.25M stimulus after HFS. (E) Release probability is significantly increased after HFS (Pre-HFS: 0.088 ± 0.008, n = 23; Post-HFS: 0.116 ± 0.013, n = 23; $p = 1.2 \cdot 10^{-3}$, paired t-test). (F) Fitted release rate constant during 0.5M HS application is significantly increased after HFS (Pre-HFS: 2.57 ± 0.21 s^{-1}, n = 26; Post-HFS: 3.12 ± 0.30 s^{-1}, n = 26; $p = 1.1 \cdot 10^{-3}$, paired t-test). (G) 'Submaximally' depleting stimuli (0.25M) also obey the relation between fraction of RRP released and release rate constant after HFS and shift upwards along the curve, confirming the observation in figure D. (H) Fraction of RRP depleted upon 0.25M HS application is significantly increased after HFS (Pre-HFS: 0.55 ± 0.05, n = 26; Post-HFS: 0.77 ± 0.04, n = 26; $p = 1.4 \cdot 10^{-7}$, paired t-test). (I) Fitted release rate constant during 0.25M sucrose application is significantly increased after HFS (Pre-HFS: 0.235 ± 0.034 s^{-1}, n = 26; Post-HFS: 0.528 ± 0.072 s^{-1}, n = 26; $p = 1.6 \cdot 10^{-5}$, paired t-test). (J) While both the release probability (figure E) and the release rate constant at 0.5M sucrose (figure F) are significantly increased due to HFS, their potentiation is not significantly correlated in WT neurons (r = 0.18, p = 0.42, n = 23). The straight line is a linear fit to the data points.

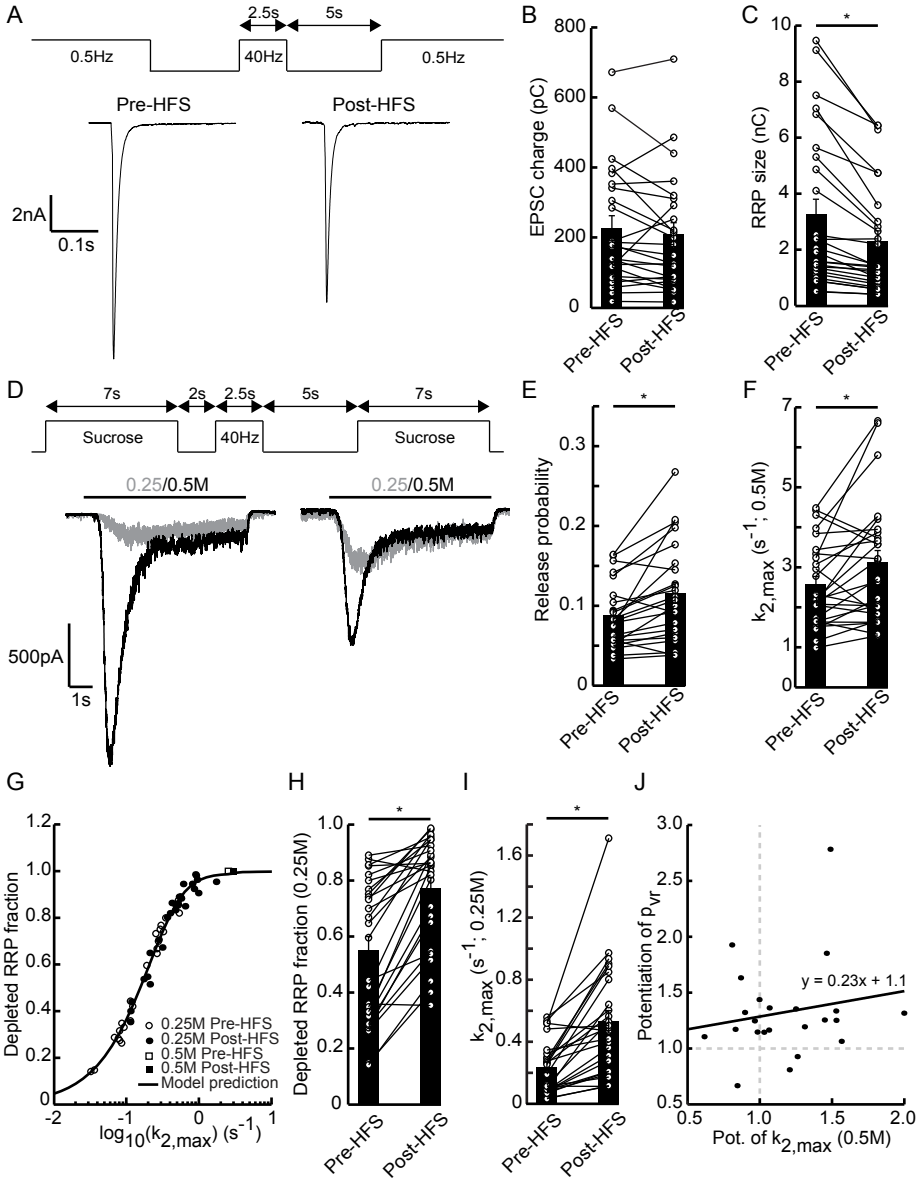
A
2.5s
5s
0.5Hz
40Hz
0.5Hz
Pre-HFS
Post-HFS
2nA
0.1s
B
EPSC charge (pC)
Pre-HFS
Post-HFS
C
RRP size (nC)
D
7s
2s
2.5s
5s
7s
Sucrose
40Hz
Sucrose
0.25/0.5M
0.25/0.5M
500pA
1s
E
Release probability
F
k2,max (s-1; 0.5M)
G
Depleted RRP fraction
0.25M Pre-HFS
0.25M Post-HFS
0.5M Pre-HFS
0.5M Post-HFS
Model prediction
log10(k2,max) (s-1)
H
Depleted RRP fraction (0.25M)
I
k2,max (s-1; 0.25M)
J
Potentiation of pvr
y = 0.23x + 1.1
Pot. of k2,max (0.5M)

assessed by application of 0.5M sucrose before and 5 seconds after HFS (fig. 5.1C–D). On average, RRP recovery was only 70%, arguing against a major role for priming in PTP. As a consequence, p_{vr} obtained by dividing the charge of the AP-induced EPSC by the charge of the RRP was potentiated by 32% (fig. 5.1E). At the same time, the kinetics of sucrose response as measured by the release rate constant $k_{2,max}$ were increased by 21% (fig. 5.1F), which corresponds to a reduction of the fusion energy barrier by 0.2RT [187].

To confirm a reduction of the fusion energy barrier after PTP, we tested whether submaximal sucrose stimuli (e.g. 0.25M) would release a larger fraction of the RRP after HFS, as predicted by our model for reduced energy barriers [187]. Indeed, in contrast to the reduced 0.5M responses, nearly all 0.25M responses were clearly potentiated 5 seconds after HFS (fig. 5.1D). Meanwhile, the relation between $k_{2,max}$ and the depleted RRP fraction found in our previous study was maintained (fig. 5.1G–H). Interestingly, $k_{2,max}$ for 0.25M responses was potentiated by 125% (fig. 5.1I), corresponding to a reduction in fusion energy barrier height by 0.8RT and differing significantly from the potentiation of 0.5M responses ($p = 2.73 \cdot 10^{-6}$, two-sample t-test).

Finally, we plotted the HFS-induced potentiation of p_{vr} versus the HFS-induced potentiation of $k_{2,max}$ of 0.5M HS responses per cell (fig. 5.1J), to study the relationship between PTP (essentially the potentiation of p_{vr}) and changes in the fusion energy barrier height. These quantities turned out to be not significantly correlated ($r = 0.18$, $p = 0.42$; $n = 23$), with most cells showing either a potentiation of p_{vr} or $k_{2,max}$, but not necessarily both at the same time. We also did not find a correlation between the potentiation of p_{vr} and the potentiation of $k_{2,max}$ of 0.25M responses ($r = -0.20$, $p = 0.35$; $n = 23$). We thus conclude that in autapses RRP recovery is incomplete 5 seconds after HFS, implying that activity-dependent priming cannot explain PTP, whereas both p_{vr} and the 'release willingness' of vesicles ($k_{2,max}$) are increased. However, the relation between the latter two parameters is unclear for individual cells, probably because of additional factors that control p_{vr} and thus PTP [47].

5.2.2 Post-tetanic reduction in fusion energy barrier does not require Synaptotagmin-1

To investigate whether the increased vesicular release probability can be attributed to an increased activation of the Ca^{2+} sensor for synchronous release, for instance through the accumulation of residual Ca^{2+}, we performed a similar set of experiments in Syt-1 KO cells. Since Syt-1 KO neurons lack fast synchronous release (fig. 5.2A) we quantified the charge of the remaining slow asynchronous component by integrating the AP-evoked current over a 100 ms period. While WT neurons showed no change (fig. 5.1A–B), Syt-1 KO neurons

displayed a significant 48% increase in amount of AP-evoked charge released 5 seconds after HFS (fig. 5.2A–B). However, as in WT cells, the recovery of the RRP 5 seconds after HFS was not complete in these neurons (78% recovery; fig. 5.2C). These findings imply that p_{vr} is even stronger potentiated in Syt-1-deficient neurons (93% increase; fig. 5.2E). The 27% potentiation of the 0.5M HS induced release rate constant $k_{2,max}$ was however remarkably similar to the WT situation (fig. 5.2F), corresponding to a 0.2RT HFS-induced reduction in fusion energy barrier height in Syt-1 KO neurons.

As in the WT situation, Syt-1 KO neurons obeyed the sigmoidal relation between depleted RRP fraction and the HS-induced release rate constant, with both quantities being increased after HFS (fig. 5.2G–H). The potentiation of $k_{2,max}$ for 0.25M responses was 84% (fig. 5.2I), corresponding to a reduction in fusion energy barrier height by 0.6RT and (again) differing significantly from the potentiation of 0.5M responses ($p = 1.14 \cdot 10^{-4}$, two-sample t-test).

Finally, we plotted the potentiation of p_{vr} against the potentiation of the 0.5M HS-induced release rate constant per cell (fig. 5.2J). This correlation appears to be significant in the Syt-1 KO situation ($r = 0.59$, $p = 2.0 \cdot 10^{-3}$, $n = 25$) — however, this is entirely due to the single outlier displaying large potentiation of both quantities: its removal ablates the correlation ($r = -0.12$, $p = 0.58$, $n = 24$). Note that while the average potentiation of $k_{2,max}$ is similar for both genotypes (WT: 1.21, Syt-1 KO: 1.27), the average potentiation of p_{vr} is much stronger in Syt-1 KO neurons (WT: 1.32, Syt-1 KO: 1.93). As in the WT situation, we also did not find a correlation between the potentiation of p_{vr} and the potentiation of $k_{2,max}$ of 0.25M responses ($r = 0.35$, $p = 0.10$; $n = 23$).

Therefore, we conclude that PTP (i.e. the potentiation of p_{vr}) occurs independently of Syt-1 and cannot be explained by any effects of accumulated global Ca^{2+} on the fast Ca^{2+} sensor, and in addition that Syt-1 does not regulate the reduction in fusion energy barrier after HFS, which was similar in both genotypes (fig. 5.1F, 5.2F). Furthermore, mechanisms other than a reduction in fusion energy barrier seem to contribute to PTP in autapses, the nature of which remains to be investigated.

5.3 Discussion

In this study we show that the fusion energy barrier is decreased, 5 seconds after HFS (fig. 5.1F, 5.2F). Furthermore, we show that PTP cannot be due to a temporarily increased RRP size (fig. 5.1C, 5.2C) which however does not imply that an increase in Ca^{2+}-dependent priming plays no role in STP [47, 166]. These findings also hold true in the absence of Syt-1; the only difference being a stronger potentiation of p_{vr} in Syt-1 KO neurons (fig. 5.1E, 5.2E). Other mechanisms are also likely to be involved since for individual cells the potentiation of

p_{vr} and $k_{2,max}$ are not significantly correlated.

5.3.1 The role of fusion energy barrier modulation in short-term plasticity

The rise in residual Ca^{2+} concentration during STP is known to enhance both the recruitment process of new vesicles, as well as the release probability in a number of preparations [48]. Recently, Ca^{2+}-dependent isoforms of protein kinase C (PKC) were identified as a Ca^{2+} sensor for PTP in the calyx of Held [205]. In another study in the same preparation, deletion of these PKCs was found to reduce PTP by 80%, which was concluded to be primarily due to their role in increasing the RRP size (inferred from charge transfer during HFS), but also due to their positive (but small) effect on the release probability [204].

The remaining PKC-independent contribution to PTP, as well as the PKC-

Figure 5.2 *(facing page)*: *The reduction of the fusion energy barrier during PTP does not require Syt-1.* (A) Typical example of action potential-evoked EPSCs, before and 5 s after HFS. Note the absence of synchronous release in the Syt-1 KO responses (red) and the increase of asynchronous release after HFS. WT responses (grey; fig. 5.1A) are reprinted for comparison. (B) Charge of AP-evoked EPSCs (integrated over 100 ms) is significantly increased after HFS (Pre-HFS: 53.2 ± 10.1 pC, n = 25; Post-HFS: 78.8 ± 13.4 pC, n = 25; $p = 1.2 \cdot 10^{-2}$, paired t-test). (C) RRP size, measured by 0.5M HS, is reduced 5 s after HFS (Pre-HFS: 1.90 ± 0.21 nC, n = 26; Post-HFS: 1.48 ± 0.17 nC, n = 26; $p = 5.2 \cdot 10^{-4}$, paired t-test). (D) Typical example of EPSCs evoked by application of 0.25M (pink) and 0.5M (red) HS to Syt-1-deficient neurons, before and 5 s after HFS. Note the relative increase of release triggered by the 0.25M stimulus after HFS. (E) Release probability is significantly increased after HFS (Pre-HFS: 0.028 ± 0.005, n = 25; Post-HFS: 0.054 ± 0.006, n = 25; $p = 2.3 \cdot 10^{-3}$, paired t-test). (F) Fitted release rate constant during 0.5M HS application is significantly increased after HFS (Pre-HFS: 1.94 ± 0.12 s^{-1}, n = 26; Post-HFS: 2.46 ± 0.19 s^{-1}, n = 26; $p = 3.3 \cdot 10^{-3}$, paired t-test). (G) 'Submaximally' depleting stimuli (0.25M) also obey the relation between fraction of RRP released and release rate constant after HFS and shift upwards along the curve, confirming the observation in figure D. (H) Fraction of RRP depleted upon 0.25M sucrose application is significantly increased after HFS (Pre-HFS: 0.57 ± 0.03, n = 24; Post-HFS: 0.78 ± 0.02, n = 24; $p = 4.6 \cdot 10^{-8}$, paired t-test). (I) Fitted release rate constant during 0.25M HS application is significantly increased after HFS (Pre-HFS: 0.238 ± 0.024 s^{-1}, n = 24; Post-HFS: 0.438 ± 0.041 s^{-1}, n = 24; $p = 1.3 \cdot 10^{-6}$, paired t-test). (J) The potentiation of the release probability and the release rate constant (at 0.5M HS) due to HFS are significantly correlated in Syt-1 KO neurons (r = 0.59, $p = 2.0 \cdot 10^{-3}$, n = 25). Removal of the outlier ablates this correlation (r = -0.12, p = 0.58, n = 24). The straight line is a linear fit to the data points.

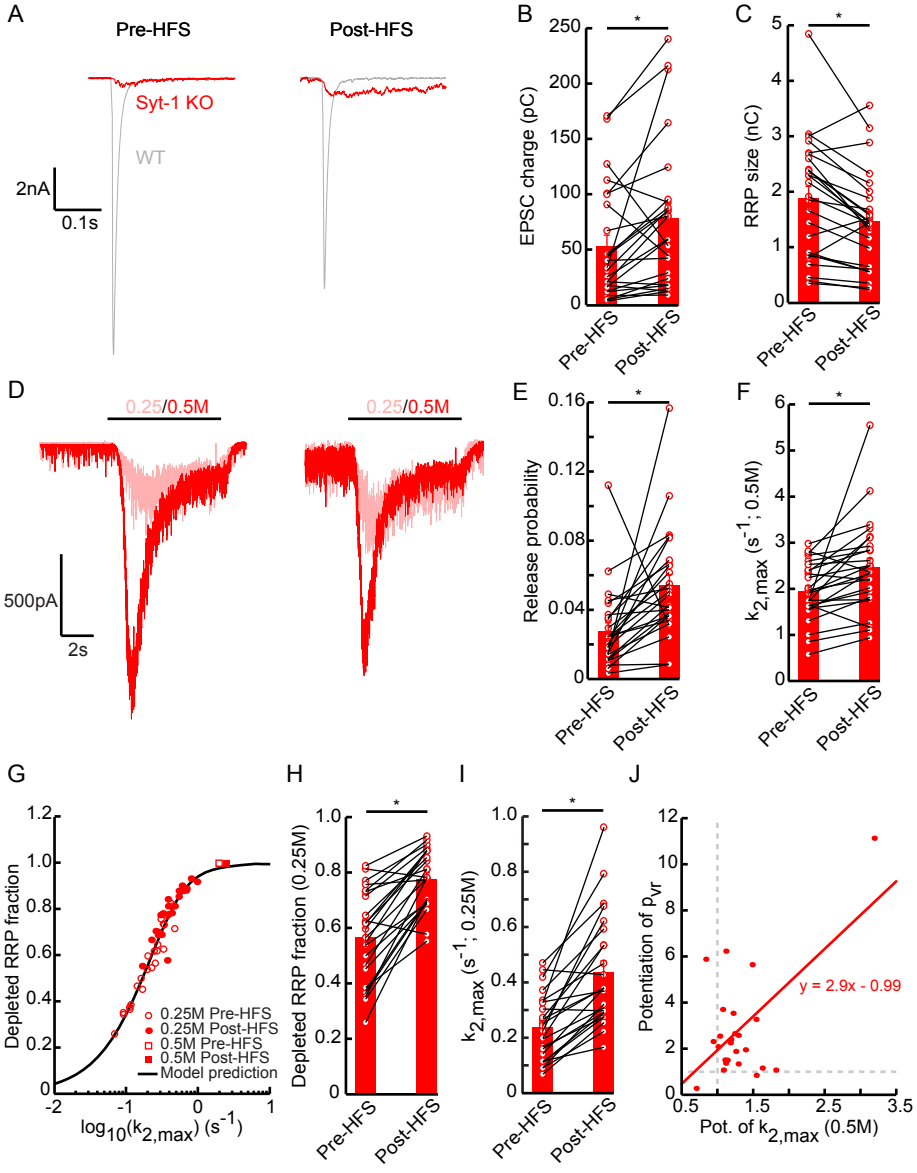
A
Pre-HFS
Post-HFS
Syt-1 KO
WT
2nA
0.1s
B
EPSC charge (pC)
Pre-HFS
Post-HFS
C
RRP size (nC)
D
0.25/0.5M
500pA
2s
E
Release probability
F
k2,max (s-1; 0.5M)
G
Depleted RRP fraction
0.25M Pre-HFS
0.25M Post-HFS
0.5M Pre-HFS
0.5M Post-HFS
Model prediction
log10(k2,max) (s-1)
H
Depleted RRP fraction (0.25M)
I
k2,max (s-1; 0.25M)
J
Potentiation of pvr
y = 2.9x - 0.99
Pot. of k2,max (0.5M)

dependent increase in release probability during PTP, could be controlled via the fusion energy barrier in a residual Ca^{2+}-dependent manner. However, the lack of correlation for individual cells between p_{vr} and release willingness ($k_{2,max}$) implies that other factors also play a role. Our interpretation of the allosteric model for Ca^{2+}-sensitivity of release provides a theoretical framework by which additive changes in the fusion energy barrier height can alter STP through an exponential effect on the release willingness parameter l_+ [76,187]. Here we provide evidence from recordings in Syt-1 KO cells that factors other than Syt-1 are responsible for the reduction of the fusion energy barrier during PTP. This rules out the possibility that the rise in residual Ca^{2+} concentration mildly activates the Ca^{2+} sensor for synchronous release, which could facilitate release during a subsequent AP-stimulus. This suggests that other proteins reduce the energy barrier, either upon direct activation by Ca^{2+}, or indirectly via Ca^{2+}-dependent intracellular pathways, such as the PKC, PLC/DAG or CaM pathways [57]. Important presynaptic proteins such as Munc18 and Munc13 have been shown to be targets of these pathways and were found to affect the energy barrier and/or STP in an activity/Ca^{2+}-dependent manner [44, 45, 79, 84, 87, 88, 166]. Further research will be needed to elucidate the contributions of each of these modulatory proteins to changes in the fusion energy barrier height during PTP.

5.3.2 The Ca^{2+}-dependent mechanism underlying the potentiation of release willingness

The post-HFS increase in release willingness presumably depends on residual Ca^{2+}, since previous studies showed that can be blocked by application of EGTA [55,56]. Also, the time constants of decay to baseline of both this potentiation effect as well as of residual Ca^{2+} are comparable to that of augmentation/PTP [55, 56, 89]. The asynchronous sensor, depending on its Ca^{2+} binding properties (see chapter 4), could therefore in principle contribute to the associated lowering of the fusion energy barrier, by retaining a 'higher/activated state' after HFS — similar to the potential PTP-mechanism involving Syt, which we ruled out in the above. An alternative candidate is the C2B domain of Munc13, which is involved in STP, affects the amount of Ca^{2+}-triggered release, but does not act as a release sensor itself [45, 89]. This scenario could be investigated by studying the amount of potentiation of p_{vr} and the co-occuring changes in release willingness in Munc13 DKO neurons expressing Ca^{2+}-insensitive copies of Munc13 (DN mutant in [45]).

5.3.3 Synaptotagmin-1 as a negative regulator of PTP

We found removal of Syt-1 to result in a stronger potentiation of p_{vr} after HFS compared to WT — in other words, the presence of Syt-1 appeared to negatively affect PTP (fig. 5.1E, 5.2E). This resulted in an increased EPSC size in Syt-1 KO neurons after HFS (fig. 5.2B), which could not be caused by an augmented RRP size (fig. 5.2C). The mechanism responsible for the enhanced potentiation of p_{vr} in Syt-1 KO neurons can be due to (1) release machinery-intrinsic properties (e.g. an alternative Ca^{2+} sensor with residual Ca^{2+}-sensitive kinetics, which becomes unclamped after removal of Syt-1 — see chapters 3-4) and/or (2) heterogeneity in vesicle positioning at the active zone combined with a loss of coupling between vesicle and Ca^{2+} channel in the absence of Syt (see chapter 6) [47, 147, 206] [3, 28-29]. In the latter situation, loss of Syt's function as a distance-regulator would result in a looser coupling and hence a lower p_{vr}, which leaves more room for potentiation.

The extent to which changes in both release machinery-intrinsic properties as well as in heterogeneity in vesicle positioning at the active zone affect STP remains an unsolved question — PTP could result from their complex interaction, combined with the PKC-dependent contribution, and Ca^{2+} and buffer dynamics [47, 205].

5.3.4 Ca^{2+}-dependent heterogeneity in potentiation of the exocytotic process

We inferred a post-HFS reduction of the fusion energy barrier from stimulations by 0.5M HS, which was subsequently confirmed by the increased fraction of RRP depleted by 0.25M stimulations (fig. 5.1D,F-I). Surprisingly, this energy barrier reduction seemed to be larger for submaximal than for maximal stimuli (fig. 5.1F,I). On the contrary, we previously found that PDBu potentiates release by lowering the fusion energy barrier by a similar amount for all HS stimuli between 0.2M and 0.5M [187]. A possible explanation could be that our method for fitting HS-induced EPSCs features a single release pathway from a homogeneous RRP [187]. All primed vesicles then have the same initial release rate constant, which would be potentiated by the same factor upon PTP. Clearly, this does not hold for the above data, for the identical design of the 0.25M and 0.5M experiments did not yield an equally potentiated release rate constant for both concentrations due to PTP (compare fig. 5.1F,I). In terms of the vesicle release machinery, this heterogeneity could result from the primed vesicles having bound a variable number of SNARE complexes and/or different zippering states of the bound SNAREs — giving a distribution of release rate constants over the primed vesicles, with 'higher SNARE states' corresponding to higher release rate constants (see the appendix to chapter 4). If we supplement this model with a

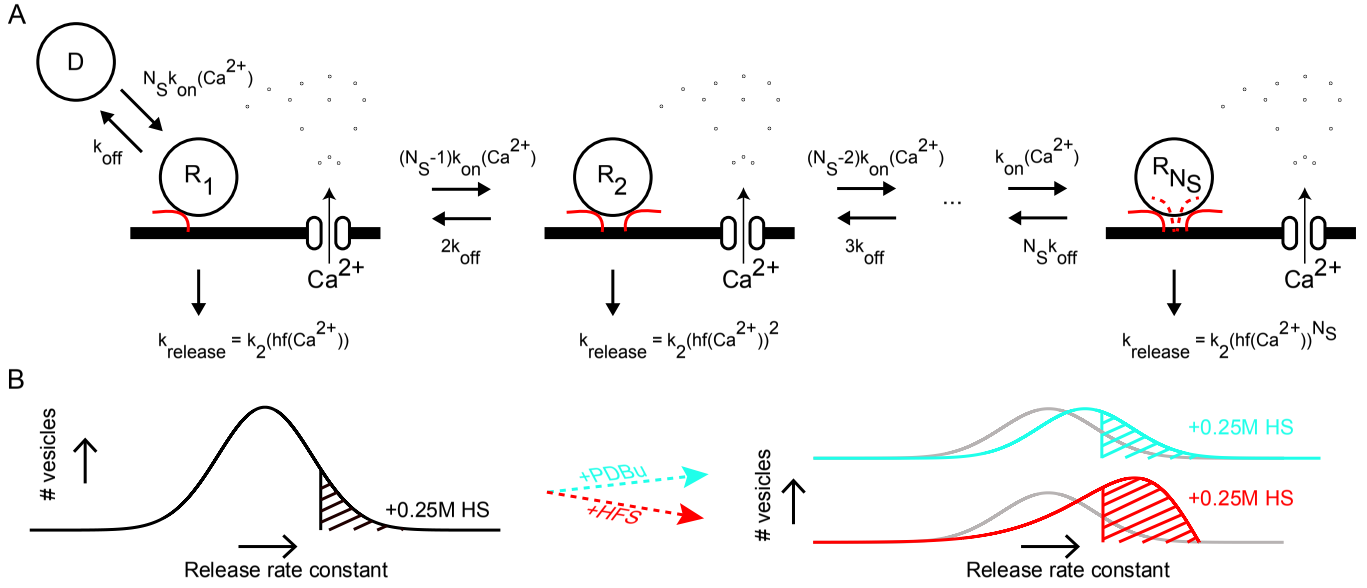

Figure 5.3: *Modeling the heterogeneous potentiation of the release rate constant after HFS.* (A) Vesicle state model describing heterogeneity in release willingness, modified from supplemental figure 4.1. The modifications include a Ca^{2+}-dependent priming rate $k_{on}(Ca^{2+})$ and a Ca^{2+}-dependent factor $f(Ca^{2+})$ multiplying the release rate to capture PTP. (B) Cartoon of distributions of the primed vesicles over the various SNARE states — resulting in heterogeneity in release rate constant across the RRP — represented as a Gaussian-like curve. The black distribution represents the nave situation, before HFS. The shaded area under all curves is the fraction of RRP depleted upon application of 0.25M HS. PDBu causes an increase in the release rate constant by the same factor for all primed vesicles (cyan) via the term k_2 in (A), resulting in a larger fraction of RRP depleted by 0.25M HS. HFS on the other hand simultaneously boosts both the priming rate and the release rate constants, resulting in a skewing of the distribution towards 'higher SNARE states' (due to increased priming) and a strong increase of the average/effective release rate constant for 0.25M HS (red). The nave distribution is shown in grey for comparison. In all situations drawn, application of 0.5M HS would deplete the entire RRP (i.e. the whole area under the curve).

Ca^{2+}-dependent priming parameter and a Ca^{2+}-dependent release rate constant to capture PTP (fig. 5.3A), this idea of heterogeneity within the RRP might provide a solution to the differential potentiating effects of PTP and PDBu as follows.

Application of 0.5M HS will release all vesicles, regardless of their initial SNARE state. Submaximal stimuli, however, only draw from states having a sufficiently high initial release rate constant (fig. 5.3B, shaded area under black distribution). Now PDBu merely boosts release via the release rate constant, thus resulting in a larger part of the RRP to be released upon 0.25M HS application (fig. 5.3B, cyan distribution), while the release rate constant is increased by the same factor as for 0.5M [187] — also in the absence of Syt-1 (chapter 3). The result of Ca^{2+}, on the other hand, is not only an increased release rate constant, but also a skewing of the primed vesicles towards 'higher SNARE states' due to Ca^{2+}-dependent priming [47, 166] (fig. 5.3B, red distribution), thus leading to a higher average/effective release rate constant (fitted to the homogeneous RRP model) and larger depleted RRP fraction for 0.25M stimuli (fig. 5.1G). The potentiation of the fitted release rate constant at 0.25M HS will, due to the skewed distribution (fig. 5.3B, red), be higher than at 0.5M HS. It should be noted, however, that this scenario only works if the rate of SNARE complex formation is not the limiting factor in the priming process (but some other step instead, such as the supply of new vesicles), since the RRP is not fully recovered 5 seconds after HFS (fig. 5.1C, 5.2C) and yet we suppose more vesicles to occupy a 'higher SNARE state' after HFS than in the naïve situation.

5.4 Materials and Methods

5.4.1 Electrophysiological recordings

Autaptic hippocampal neurons from Synaptotagmin-1 null mice or wild-type littermates were grown for 14–18 days on glia island cultures before measuring. Syt-1 knockdown cells were obtained by infecting cells with a LIP virus at DIV 2-3. Whole-cell voltage-clamp recordings ($V_m = -70mV$) were performed at room temperature with borosilicate glass pipettes (2.5–4.5 mOhm) filled with 125mM K^+-gluconic acid, 10mM NaCl, 4.6mM $MgCl_2$, 4mM K_2-ATP, 15mM creatine phosphate, 10U/ml phosphocreatine kinase and 1mM EGTA (pH 7.30). External solution contained the following (in mM):10 HEPES, 10 Glucose, 140 NaCl, 2.4 KCl, 4 $MgCl_2$ and 4 $CaCl_2$ (pH = 7.30, 300 mOsmol). Recordings were acquired with an Axopatch 200A amplifier (Molecular Devices), Digidata 1322A and Clampex 9.0 software (Molecular Devices). After whole cell mode was established, only cells with a leak current of <250 pA were accepted for analysis.

Ca^{2+}-independent vesicle release was evoked by hypertonic solutions consisting of external solution containing 250 or 500mM sucrose. Gravity infused external solution was alternated with 7 seconds of perfusion with hypertonic solution by switching between barrels within a custom-made tubing system (FSS standard polyamine coated fused silica capillary tubing, ID 430 µm, OD550 µm, Postnova analytics) attached to a perfusion Fast-Step delivery system (SF-77B, Warner instruments corporation) and directed at the neuron. Using this system, solutions can be switched within milliseconds. Solution flow was controlled with an Exadrop precision flow rate regulator (B. Braun) to assure all sucrose solutions flowed with a rate of 0.5ml/min despite differences in viscosity. Offline analysis of electrophysiology was performed using Clampfit v9.0 (Axon Instruments), Axograph X (Axograph Scientific), and custom-written software routines in Matlab 7.10.0 or R2010a (Mathworks). Analysis and fitting of EPSCs evoked by application of hypertonic sucrose was performed as described in [187].